Supporting Information Appendix for:

# Structural differences in amyloid-β fibrils from brains of non-demented elderly individuals and Alzheimer's disease patients

Ujjayini Ghosh[1,2], Wai-Ming Yau[1], John Collinge[3], and Robert Tycko[1*]

[1]Laboratory of Chemical Physics, National Institute of Diabetes and Digestive and Kidney Diseases, National Institutes of Health, Bethesda, MD 20892-0520, USA
[2]Department of Chemistry, Michigan State University, East Lansing, MI 48824, USA
[3]MRC Prion Unit and Institute of Prion Diseases, University College London, London W1W 7FF, UK

[*]corresponding author: Dr. Robert Tycko, National Institutes of Health, Building 5, Room 409, Bethesda, MD 20892-0520, USA. email: robertty@mail.nih.gov; phone: 301-402-8272

---

## SI Methods

*Selection of tissue samples*

Eight samples of frozen mid-frontal lobe tissue (0.5-0.6 g each) were generously supplied by the Rush Alzheimer's Disease Center (RADC) from the Religious Orders Study (ROS) (1). Samples were selected from subjects with a final consensus cognitive diagnosis value of 1 ("cogdx" variable in the RADC nomenclature), indicating no cognitive impairment, and with high cortical Aβ levels according to IHC analyses ("amyloid" and "amyloid_mf" variables). IHC amyloid and amyloid_mf levels were 8.2 ± 1.6 and 12.0 ± 3.9 (mean ± standard deviation) for the selected samples, respectively, compared with 2.2 ± 2.8 and 3.1 ± 4.1 for the entire ROS data set with cogdx = 1 (n = 222 as of April 2019). Age at death for the selected samples was 89.8 ± 5.7 years, compared with 85.2 ± 6.8 years for the entire ROS data set with cogdx = 1. Selected samples were from four male and four female subjects. Apolipoprotein E genotypes were E3/E3 for all samples, except E3/E4 for subject 3. Other characteristics are listed in Table S1. Although the subjects were not cognitively impaired according to the RADC assessments, Braak stages, CERAD scores, and NIA Reagan scores, which are post-mortem measures of neuropathology, indicated the presence of neurofibrillary tangles and neuritic plaques with levels and distributions similar to those found in AD patients. For subjects in the entire ROS data set with amyloid_mf ≥ 7.84, the mean cogdx value was 3.31 on a scale from 1 to 4.

t-AD and PCA-AD tissue samples were obtained from the Medical Research Council Prion Unit and the Queen Square Brain Bank for Neurological Disorders of the University College London Institute of Neurology, as described previously by Qiang *et al*. (2). These samples were from patients with clinical diagnoses of Alzheimer's disease (t-AD1 through t-AD6), posterior cortical atrophy or corticobasal syndrome (PCA-AD1 and PCA-AD2), or biparietal AD or dementia with Lewy Bodies (PCA-AD3). All t-AD and PCA-AD patients had pathological diagnoses of Alzheimer's disease, with Braak stage 6 (no Braak stage was reported for PCA-AD2). Ages at onset and at death were in the 51-65 year and 62-79 year ranges, respectively. Clinical durations were 5-21 years.

*Preparation of amyloid-containing extract*

Amyloid-containing extracts from cortical tissue samples were prepared with the method originally described by Lu *et al*. (3) and used by Qiang *et al*. (2), with minor modifications to accommodate the smaller quantities of tissue available from RADC (0.5-0.6 g per tissue sample, rather than 2-3 g). The eight tissue samples were processed in two sets of four. In each set, tissue samples were thawed, placed in 15 ml polypropylene tubes containing 5 ml of buffer A (10 mM Tris-HCl, pH 7.5, 0.25 M sucrose, 3 mM ethylenediaminetetraacetic acid (EDTA), and 0.1% w/v $NaN_3$) and one half tablet of Roche Complete Protease Inhibitor. Mixtures were homogenized thoroughly (IKA Ultra-Turrax T18 homogenizer), then rotated end-over-end overnight at 4° C. Sucrose concentrations were then increased to 1.2 M by addition of 4.1 g of sucrose and buffer A to a final volume of 11 ml. Mixtures were then transferred to ultracentrifuge tubes (Beckman Coulter model 344060) and spun at 220,000×g (Beckman Coulter SW40Ti rotor) for 60 min at 4° C. Top layers of fat and supernatant solutions were removed. Pellets were resuspended in 11 ml of buffer B (10 mM Tris-HCl, pH 7.5, 1.9 M sucrose, 3 mM EDTA, and 0.1% w/v $NaN_3$), then centrifuged again at 220,000×g for 60 min at 4° C. Top layers, containing the desired material, were transferred to 15 ml polypropylene tubes, resuspended in 10 ml of Tris-HCl buffer (50 mM, pH 8.0) and spun at 11,000×g (Beckman Coulter F0685 rotor) for 15 min at 4° C. Supernatants were removed and pellets were frozen in liquid nitrogen for overnight storage at -25° C. On the following day, pellets were thawed and resuspended in 10 ml of Tris-HCl buffer with 2 mM $CaCl_2$. DNAse I was added from a 5 mg/ml stock solution to a final concentration of 10 μg/ml. After incubation with orbital mixing for 60 min at room temperature, suspensions were pelleted again at

11,000×g for 15 min. Pellets were resuspended in 2.0 ml of buffer C (10 mM Tris-HCl, pH 7.5, 1.3 M sucrose, 3 mM EDTA, 0.1% w/v $NaN_3$, and 1% w/v sodium dodecyl sulfate), spun for 10 min at 1500×g, then transferred to ultracentrifuge tubes (Beckman Coulter model 344057). After adding buffer C to a total volume of 4.5 ml, suspensions were spun at 350,000×g for 30 min at 4° C (Beckman Coulter TLA-100.4 rotor). Top layers of fat and the supernatant were removed. Residual buffer C was removed by resuspending the pellets in deionized water and spinning again at 350,000×g for 30 min at 4° C, with two repetitions. Finally, pellets were resuspended in approximately 0.5 ml of 10 mM sodium phosphate buffer, pH 7.4, with 0.01% $NaN_3$. Suspensions from each tissue sample were divided into two equal volumes (one for Aβ40, one for Aβ42), frozen in liquid nitrogen, and stored at -25° C.

*Aβ peptide synthesis*

Aβ40 with uniformly $^{15}N$,$^{13}C$-labeled F19, V24, G25, S26, A30, I31, L34, and M35 was synthesized on a nominal 0.1 mmol scale using fluorenylmethyloxycarbonyl (Fmoc) chemistry with N,N'-diisopropylcarbodiimide/OxymaPure activation on a Biotage Initiator+ Alstra solid phase peptide synthesizer. Fmoc-Val-NovaSyn-TGA resin was obtained from Sigma-Aldrich with substitution of 0.18 mEq/g. Actual resin mass was 450 mg, corresponding to 0.08 mmol. Unlabeled residues were double-coupled with a five-fold excess of Fmoc-amino acid and DIC/OxymaPure in N-methyl-2-pyrrolidone for 10 min at 75° C, except that Fmoc-Arg(Pbf)-OH was double-coupled for 15 min at 75° C and Fmoc-His(Boc)-OH was double-coupled for 15 min at 50° C. For isotopically labeled residues, a three-fold excess of the labeled Fmoc-amino acid was single-coupled for 20 min at 75° C, followed by single-coupling with a five-fold excess of unlabeled Fmoc-amino acid for 5 min at 75° C. After each Fmoc-amino acid was double-coupled, capping was performed with acetic anhydride/N,N-diisopropylethylamine to block the ends of unreacted chains and thereby minimize deletion impurities in the final product. Deprotection with 20% piperidine in dimethylformamide was performed at room temperature in three steps, for 3, 10 and 10 min. Cleavage from the synthesis resin was performed with a standard cocktail (trifluoroacetic acid/phenol/thioanisole/1,2-ethanedithiol/water, 10 ml/0.75 g/0.5 ml/0.25 ml/0.5 ml) for 2.0 h. During the last 15 min of cleavage, 200 mg of tetrabutylammonium bromide was added to reduce any oxidized methionine at M35 of the Aβ40 sequence. After filtering and washing

the resin with trifluoroacetic acid, the crude product was precipitated by cold methyl tert-butyl ether and the pellet was further washed with cold methyl tert-butyl ether twice. The final product was purified by preparative high-performance liquid chromatography (HPLC) on a Zorbax 300SB-C3 reverse-phase column (Agilent Technologies). Aβ42 with uniformly $^{15}N$,$^{13}C$-labeled F19, G25, A30, I31, L34, and M35 was prepared in a similar manner, except that H-Ala-HMPB-ChemMatrix resin was obtained from Sigma-Aldrich and its substitution was determined to be 0.48 mEq/g using the method described by Eissler *et al*. (4)

*Seeded growth of Aβ fibrils*

The seeded growth protocol illustrated in Fig. 1a was used to amplify Aβ fibril structures from cortical tissue extract and to generate isotopically labeled fibrils, as required for solid state NMR measurements. Extract in phosphate buffer (10 mM sodium phosphate, pH 7.4, 0.01% w/v $NaN_3$), prepared as described above, was thawed and sonicated for 20 min (Branson S-259A sonifier with tapered 1/8" microtip horn, lowest power, 10% duty factor). Isotopically labeled Aβ40 (Aβ42) was fully dissolved in DMSO to a concentration of 5.0 mM. The volume of the extract solution was increased to 0.47 ml (1.8 ml) by adding phosphate buffer. An aliquot of the DMSO solution containing 0.2 mg of Aβ40 (Aβ42) was added to produce a 100 μM (25 μM) concentration of soluble Aβ40 (Aβ42). After immediate vortexing, fibrils were allowed to grow quiescently at 24° C for 4.0 h. Grids for negative-stain TEM were prepared to verify seeded fibril growth. The entire fibril solution was then sonicated for 10 min. Phosphate buffer was added to increase the volume to 3.5 ml (13.6 ml) and an aliquot of the DMSO solution containing 1.3 mg of Aβ40 (Aβ42) was added. After immediate vortexing, fibril growth was allowed to continue quiescently at 24° C for 18-24 h. TEM grids were prepared again. The entire solution was then incubated overnight with intermittent sonication (one 10 s pulse per hour, Qsonica model Q55 sonicator, 1/8" horn, power level 20, controlled by Omega PTC-16 timer). Quiescent incubation then proceeded for an additional 24-48 h at 24° C before fibrils were pelleted at 220,000×g for at least 4 h, resuspended in deionized water, pelleted again, lyophilized, and stored at -25° C.

Unseeded Aβ40 fibrils for Figs. 2 and S3 were prepared by adding 4.0 mg of DMSO-solubilized Aβ40 to phosphate buffer to produce an Aβ40 concentration of 120 μM, then incubating at 24° C for 7 days with orbital agitation (Stuart SSM1 orbital shaker, 60 revolutions

per minute). Fibrils were pelleted, resuspended in deionized water, pelleted again, lyophilized, and stored at -25° C. Unseeded Aβ42 fibrils for Figs. 3 and S3 were prepared similarly, but at an Aβ42 concentration of 50 μM (3.9 mg of Aβ42) and with incubation for 13 days.

For control experiments in Fig. S8, fibrils were grown in the presence of extract from amyloid-free occipital lobe tissue as previously described (2). Aβ40 and Aβ42 fibrils were allowed to grow quiescently for 168 h and 48 h, respectively, followed by a 24 h period of intermittent sonication and a final 72 h period of quiescent incubation. Although TEM images showed no fibrils after the initial 4 h incubation periods, abundant fibrils were observed after the 168 h and 48 h periods, as expected from spontaneous nucleation and growth at the 100 μM and 25 μM peptide concentrations, respectively. The occipital lobe tissue was obtained from the autopsy of an 86 year old female who had died from cardiac arrest.

*Electron microscopy*

TEM images were obtained with an FEI Morgagni microscope, operating at 80 keV. Fibril solutions were diluted in deionized water by a factor of 5-10. Aliquots (8-10 μl) were then adsorbed for 1-3 min on glow-discharged TEM grids. For Aβ40 fibrils, 300 mesh carbon coated Quantifoil S200/700 grids were used. For Aβ42 fibrils, grids consisting of carbon films supported by lacey carbon on 300 mesh copper were used. Grids were blotted, rinsed twice with 8-10 μl of deionized water, then stained with an 8-10 μl aliquot of 2% w/v uranyl acetate for 15-30 s. Grids were then blotted and allowed to dry in air. Images were recorded with a side-mounted Advantage HR camera (Advanced Microscopy Techniques).

*Solid state NMR spectroscopy*

For solid state NMR measurements, lyophilized fibrils were packed into 1.8 mm magic-angle spinning (MAS) rotors, then rehydrated by addition of excess 10 mM phosphate buffer, pH 7.4, centrifugation of the MAS rotor at 16,000 × g for 15-30 min, and blotting with tissue paper to remove excess buffer before sealing with the standard rotor end cap. Solid state NMR spectra of Aβ40 fibrils were obtained at 14.1 T and 17.5 T (599.1 MHz and 746.4 MHz $^{1}$H NMR frequencies, respectively), using Varian InfinityPlus spectrometers and 1.8 mm MAS NMR probes produced by the laboratory of Dr. Ago Samoson (Tallinn University of Technology, Estonia). MAS

frequencies were 13.60 kHz at 14.1 T and 17.00 kHz at 17.5 T. Sample temperatures were 26 ± 2° C.

2D $^{13}C$-$^{13}C$ spectra of Aβ40 fibrils used 2.65 ms or 2.82 ms finite-pulse radio-frequency-driven recoupling (5, 6) periods between $t_1$ and $t_2$ periods in measurements at 14.1 T or 17.5 T, respectively, with $^{13}C$ π pulses equal to 22 μs or 18 μs at a carrier frequency of 30 ppm. Maximum $t_1$ values were 5.0 ms or 4.0 ms, respectively. 2D $^{15}N$-$^{13}C$ spectra of Aβ40 fibrils used 4.0 ms $^{15}N$-$^{13}C$ cross-polarization periods between $t_1$ and $t_2$ periods, with maximum $t_1$ values were 6.0 ms or 4.8 ms, respectively. $^{1}H$ decoupling fields were approximately 100 kHz in all spectra, with two-pulse phase modulation (TPPM) (7) in $t_1$ and $t_2$. Delays between scans were 1.0 s. Total measurement times were 8-39 h for 2D $^{13}C$-$^{13}C$ spectra and 19-75 h for 2D $^{15}N$-$^{13}C$ spectra of RADC Aβ40 fibrils.

Measurements on Aβ42 fibrils were performed at 14.1 T, using a Tecmag Redstone spectrometer. Other measurement conditions were the same as for Aβ40 fibrils, except that the maximum $t_1$ values were 4.0 ms and 10.0 ms for 2D $^{13}C$-$^{13}C$ and 2D $^{15}N$-$^{13}C$ spectra, respectively, and delays between scans were 0.8 s. Total measurement times were 40-154 h for 2D $^{13}C$-$^{13}C$ spectra and 63-245 h for 2D $^{15}N$-$^{13}C$ spectra of RADC Aβ42 fibrils. 1D solid state $^{13}C$ NMR spectra of all samples used 100 kHz TPPM decoupling.

2D spectra were processed with NMRPipe (8), using 0.66 ppm Gaussian apodization in $^{13}C$ dimensions and 1.65 ppm Gaussian apodization in $^{15}N$ dimensions. 2D spectra in Figs. 2, 3, 6, 7, and S4-S9 were plotted with Sparky (https://www.cgl.ucsf.edu/home/sparky/). 1D $^{13}C$ spectra in Fig. S3 were processed with 0.33 ppm Gaussian apodization. $^{13}C$ chemical shifts are relative to 2,2-dimethyl-2-silapentane-5-sulphonic acid (DSS), taking the carboxylate $^{13}C$ NMR frequency of an external standard of 1-$^{13}C$-L-alanine powder to be 179.65 ppm. $^{15}N$ chemical shifts are relative to liquid ammonia, with 0.00 ppm taken to be 0.402907564 times the carboxylate $^{13}C$ NMR frequency of 1-$^{13}C$-L-alanine powder.

*RMSD analyses*

RMSD analyses were performed as described by Qiang *et al*. (2). Regions of 2D $^{13}C$-$^{13}C$ spectra from 5.0 ppm to 75.0 ppm in both dimensions and regions of 2D $^{15}N$-$^{13}C$ spectra from 100.0 ppm to 140.0 ppm in the $^{15}N$ dimension and from 35.0 ppm to 70.0 ppm in the $^{13}C$ dimension were first converted to text files with the pipe2txt command of NMRPipe. The Fortran95 program

compare_spectra.f95 (available upon request) was then used to calculate the RMSD values that are displayed in Fig. 4. Within this program, 2D spectra were interpolated onto a common grid of frequency points, with 0.2 ppm increments in both dimensions. For each pair of 2D spectra $S_1(\nu_1,\nu_2)$ and $S_2(\nu_1,\nu_2)$, root-mean-squared noise levels were determined from regions that were devoid of crosspeak signals. Points $(\nu_{1k},\nu_{2k})$ where the signal was more than 4.0 times the noise level in either spectrum were selected. For 2D $^{13}C$-$^{13}C$ spectra, signal points that were within 5.0 ppm of the diagonal (*i.e.*, $|\nu_1 - \nu_2| < 5.0$ ppm) were excluded. The RMSD value was then calculated as $\sqrt{M\sum_{k=1}^{M}[S_1(\nu_{1k},\nu_{2k}) - q_{12}S_2(\nu_{1k},\nu_{2k})]^2} \Big/ \sum_{k'=1}^{M}[S_1(\nu_{1k'},\nu_{2k'}) + q_{12}S_2(\nu_{1k'},\nu_{2k'})]$, where M is the number of selected points and $q_{12}$ is the optimal scaling factor applied to $S_2(\nu_1,\nu_2)$, *i.e.*, the scaling factor that minimizes the RMSD value. Calculated this way, each RMSD value is normalized to the average signal amplitude in the two spectra. In addition, displacements of $S_2(\nu_1,\nu_2)$ from -0.5 ppm to +0.5 ppm were tested in increments of 0.1 ppm and the smallest RMSD value was retained, to account for possible discrepancies in chemical shift referencing between the two 2D spectra.

We emphasize that all points that were above 4.0 times the root-mean-squared noise level in either of the two 2D spectra (except points close to the diagonal in the case of $^{13}C$-$^{13}C$ spectra) were used to calculate the RMSD value for a given pair of spectra, according to the mathematical expression given above. Positions of crosspeaks were not identified explicitly. This approach allows RMSD values to be calculated without assumptions regarding the shapes or widths of the crosspeaks and without assuming that a specific number of crosspeaks exist in the 2D spectra. Scaling factors $q_{12}$ are determined by the exact formula $q_{12} = \sum_{k=1}^{M} S_1(\nu_{1k},\nu_{2k})S_2(\nu_{1k},\nu_{2k}) \Big/ \sum_{k'=1}^{M} S_2(\nu_{1k'},\nu_{2k'})S_2(\nu_{1k'},\nu_{2k'})$.

*Principal component analyses*

Principal component analyses were also performed as described by Qiang *et al*. (2), using the Fortran95 program compare_spectra_pca.f95 (available upon request). Within this program, all 2D spectra were interpolated onto the same grid, root-mean-squared noise levels were determined, and signal points were selected as described above for RMSD analyses, with the selected points including all frequency pairs $(\nu_{1k},\nu_{2k})$ where signals in any of the 2D spectra were

greater than 4.0 times the noise level. Each 2D spectrum was then represented as an M-dimensional vector, where M is the number of selected points. Principal component spectra (Figs. S8 and S9), principal values (Fig. S10), and coefficients (Fig. 5) were calculated by applying singular value decomposition to the set of L M-dimensional vectors, where L is the number of 2D spectra, using the sgesvd routine of LAPACK.

*Statistics*

Igor Pro 6.37 (Wavemetrics, Inc.) was used to perform Kalmogorov-Smirnov and Wilcoxon-Mann-Whitney tests on sets of RMSD values and principal component coefficients. Origin 2020b (OriginLab Corp.) was used to calculate averages and standard deviations and to perform Welch's t-test. Origin 2020b was also used to create heat maps and plots in Figs. 4, 5, S3, and S10.

**SI references**


1. Bennett, D.A., *et al.*, Religious orders study and Rush memory and aging project. *J. Alzheimers Dis.* **64**, S161-S189 (2018).
2. Qiang, W., Yau, W.M., Lu, J.X., Collinge, J., and Tycko, R., Structural variation in amyloid-β fibrils from Alzheimer's disease clinical subtypes. *Nature* **541**, 217-221 (2017).
3. Lu, J.X., *et al.*, Molecular structure of β-amyloid fibrils in Alzheimer's disease brain tissue. *Cell* **154**, 1257-1268 (2013).
4. Eissler, S., *et al.*, Substitution determination of Fmoc-substituted resins at different wavelengths. *J. Pept. Sci.* **23**, 757-762 (2017).
5. Ishii, Y., $^{13}C$-$^{13}C$ dipolar recoupling under very fast magic angle spinning in solid-state nuclear magnetic resonance: Applications to distance measurements, spectral assignments, and high-throughput secondary-structure determination. *J. Chem. Phys.* **114**, 8473-8483 (2001).
6. Bennett, A.E., *et al.*, Homonuclear radio frequency-driven recoupling in rotating solids. *J. Chem. Phys.* **108**, 9463-9479 (1998).
7. Bennett, A.E., Rienstra, C.M., Auger, M., Lakshmi, K.V., and Griffin, R.G., Heteronuclear decoupling in rotating solids. *J. Chem. Phys.* **103**, 6951-6958 (1995).
8. Delaglio, F., *et al.*, Nmrpipe: A multidimensional spectral processing system based on Unix pipes. *J. Biomol. NMR* **6**, 277-293 (1995).

**Table S1**: Characteristics of RADC subjects

| RADC subject | APOE genotype | age at death (yr) | gender | Braak stage[1] | CERAD score[2] | NIA Reagan score[3] | mid-frontal amyloid[4] | cortical amyloid[5] | mid-frontal NFT[6] | cortical NFT[7] |
|---|---|---|---|---|---|---|---|---|---|---|
| 1 | E3/E3 | 89.9 | male | 5 | 2 | 2 | 8.84 | 7.85 | 0.27 | 13.43 |
| 2 | E3/E3 | 86.5 | male | 5 | 2 | 2 | 10.32 | 7.06 | 0.08 | 10.44 |
| 3 | E3/E4 | 85.1 | female | 4 | 2 | 2 | 17.82 | 8.72 | 0.60 | 3.23 |
| 4 | E3/E3 | 86.9 | male | 4 | 1 | 2 | 10.35 | 7.16 | 0.00 | 5.80 |
| 5 | E3/E3 | 83.0 | male | 5 | 1 | 1 | 17.76 | 10.88 | 2.99 | 11.60 |
| 6 | E3/E3 | 91.9 | female | 3 | 2 | 2 | 13.72 | 9.91 | 0.02 | 2.67 |
| 7 | E3/E3 | 99.7 | female | 4 | 1 | 2 | 9.54 | 6.34 | 0.06 | 3.16 |
| 8 | E3/E3 | 95.2 | female | 5 | 1 | 1 | 7.84 | 7.36 | 0.53 | 11.52 |

[1]Progression of neurofibrillary tangle (NFT) pathology, from the transentorhinal region (stage 1) to the entire neocortex (stage 6).
[2]Likelihood of AD, based on neuritic plaque density: 1 = definite; 2 = probable.
[3]Likelihood of AD, based on neurofibrillary tangles (NFTs) and neuritic plaques: 1 = high likelihood; 2 = intermediate likelihood.
[4]Percentage of midfrontal cortex occupied by Aβ, based on immunohistochemistry (IHC). Mean, standard deviation, maximum, and median values in the entire ROS data set (n=761 as of April 2019) are 4.38, 4.82, 30.35, and 2.81, respectively.
[5]Percentage of cortex occupied by Aβ, based on IHC. Mean, standard deviation, maximum, and median values in the entire ROS data set are 3.36, 3.45, 19.93, and 2.43, respectively.
[6]NFT burden in midfrontal cortex, based on IHC. Mean, standard deviation, maximum, and median values in the entire ROS data set are 2.14, 7.29, 72.71, and 0.02, respectively.
[7]NFT burden in cortex, based on IHC. Mean, standard deviation, maximum, and median values in the entire ROS data set are 6.88, 8.48, 61.01, and 3.98, respectively.

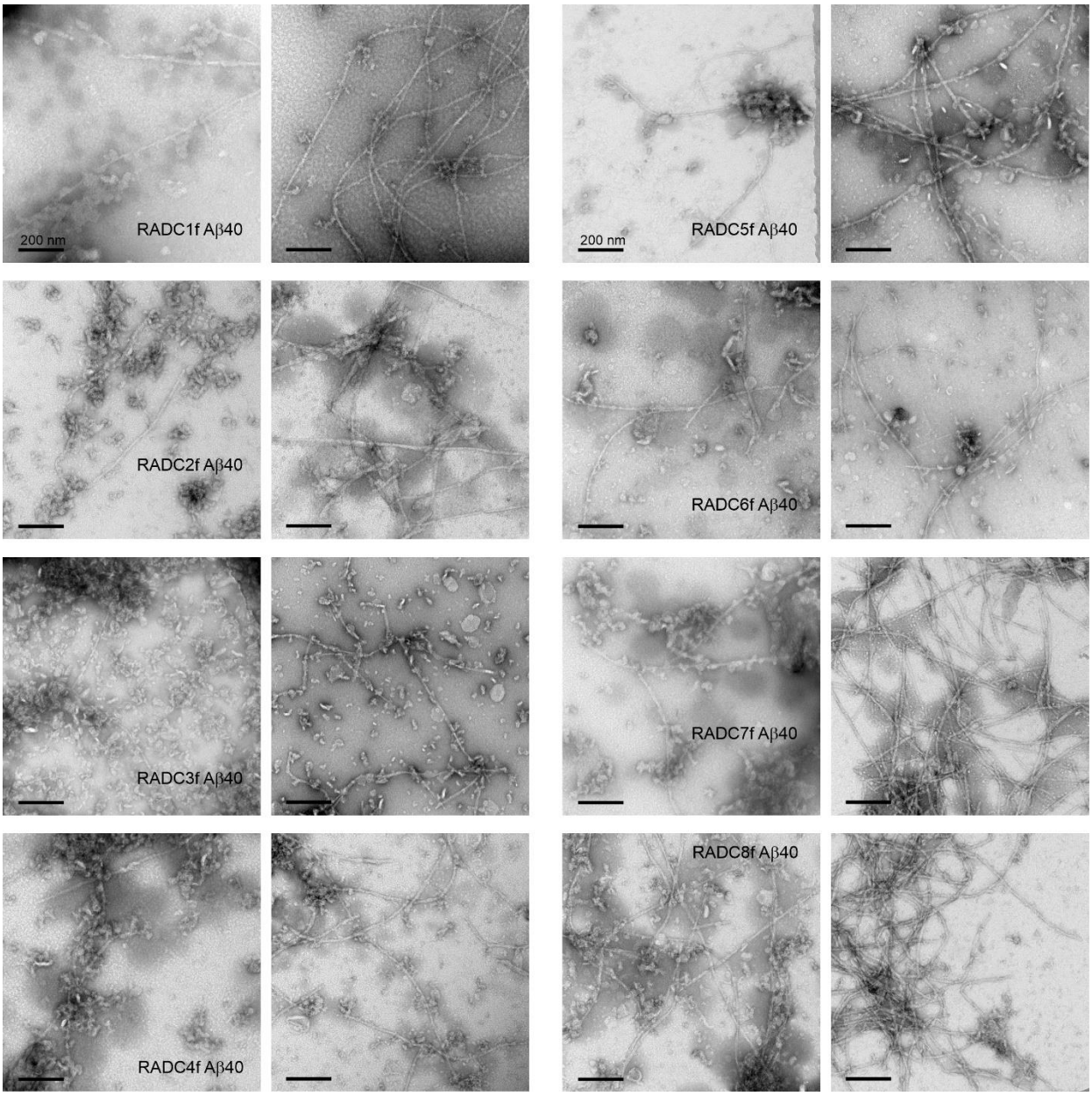


**Figure S1**: TEM images of negatively stained Aβ40 fibrils prepared by seeded growth from amyloid-enriched extracts of frontal lobe tissue of RADC subjects 1-8. For each subject, the image on the left was obtained after the initial 4 h incubation step (see Fig. 1a). The image on the right was obtained after the subsequent 18-24 h incubation step. All scale bars are 200 nm.

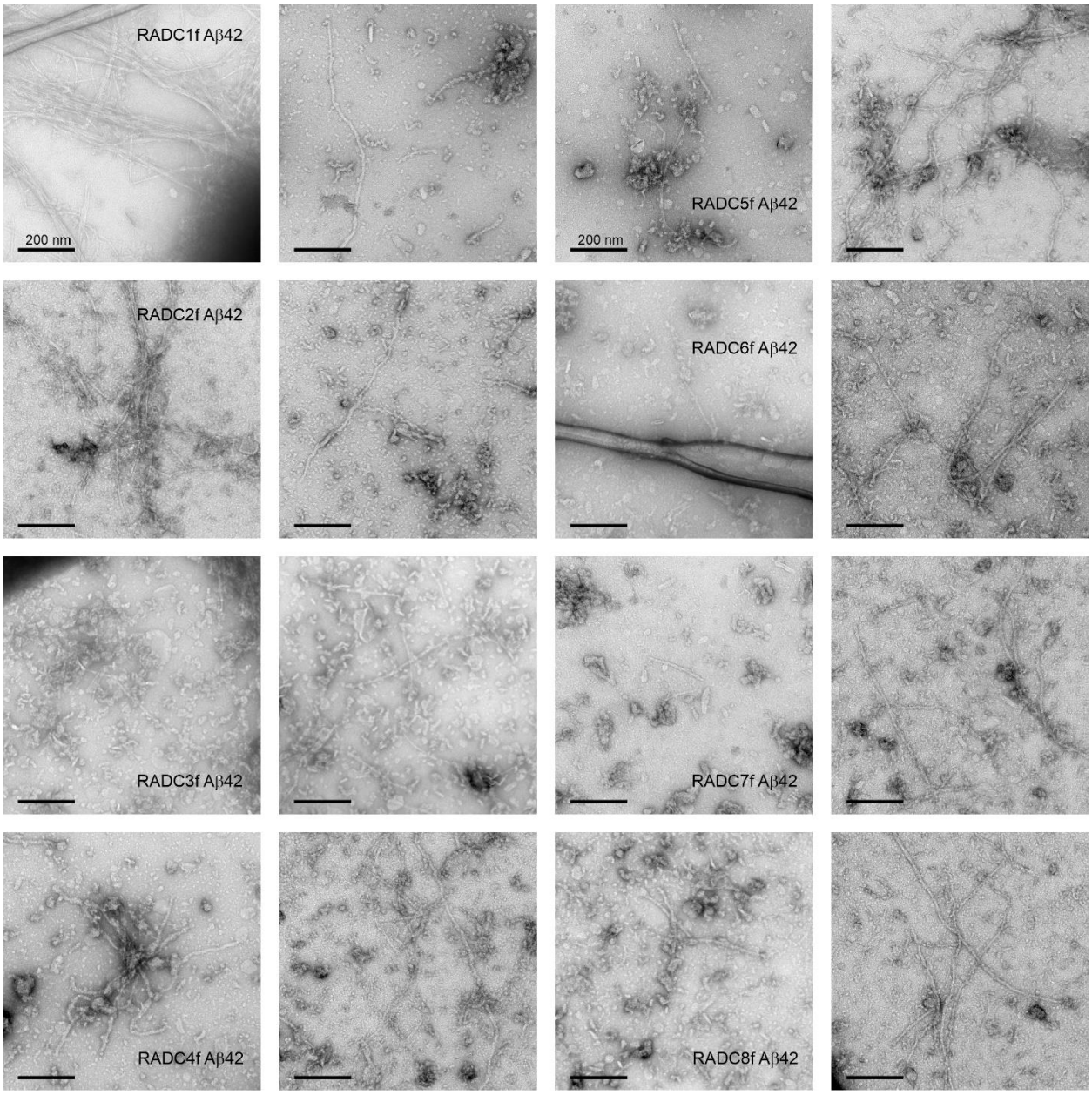


**Figure S2**: Same as Fig. S1, but for Aβ42 fibrils.

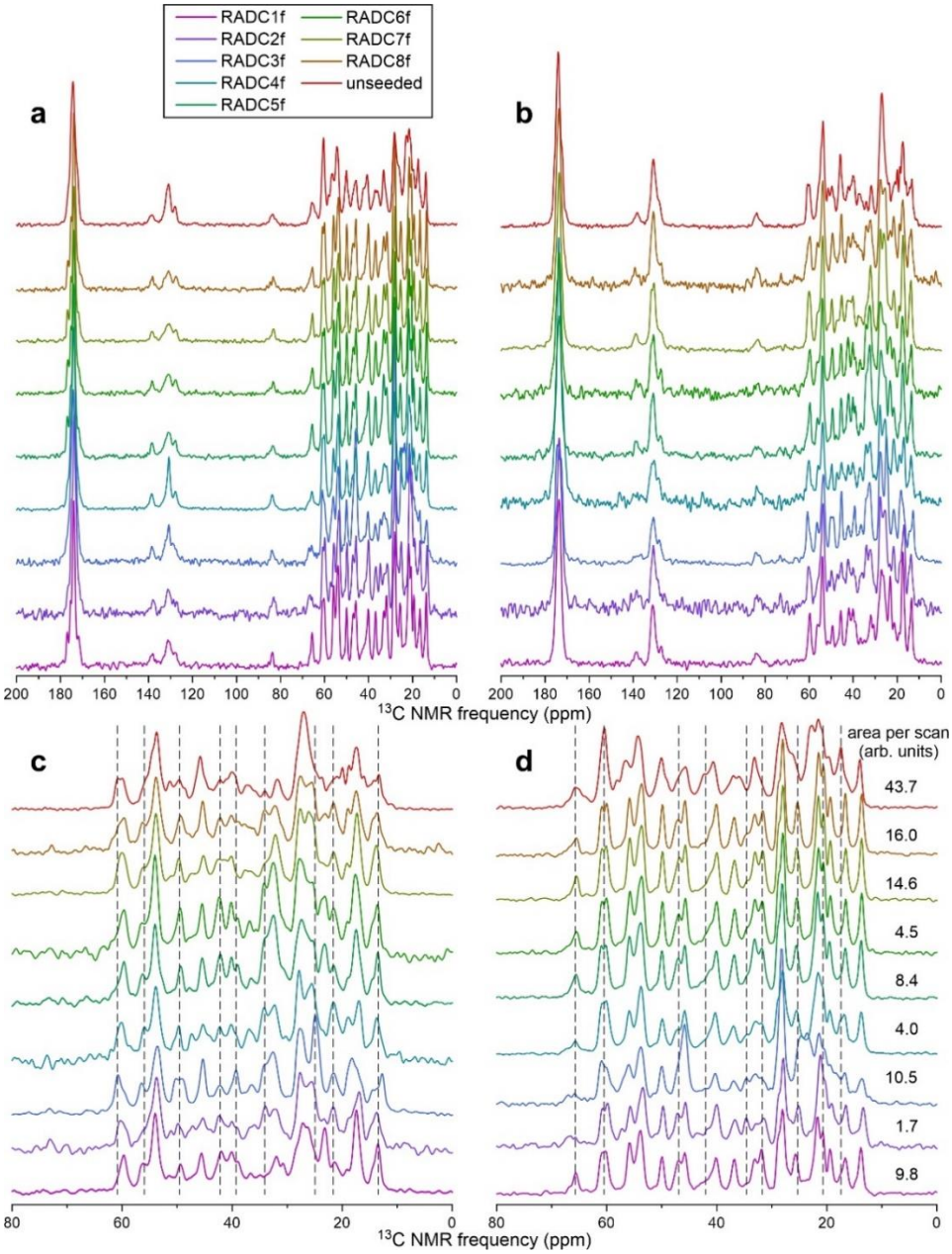


**Figure S3**: 1D $^{13}$C solid state NMR spectra of fibrils prepared by seeded growth from amyloid-enriched extracts of frontal lobe tissue of RADC subjects 1-8 and of fibrils grown *in vitro* without seeding. (a) Spectra of Aβ40 fibrils with uniform $^{15}$N,$^{13}$C-labeling of F19, V24, G25, S26, A30, I31, L34, and M35. (b) Spectra of Aβ42 fibrils with uniform $^{15}$N,$^{13}$C-labeling of F19, G25, A30, I31, L34, and M35. (c,d) Expansions of the aliphatic region of the spectra in panels A and B, respectively. Vertical dashed lines indicate some of the positions where spectral intensities vary. Total aliphatic signal areas, adjusted for differences in signal averaging, are shown in panel d to indicate differences in the quantities of Aβ42 fibrils that were generated with the same seeded growth protocol, starting with approximately the same mass of frontal lobe tissue. For ease of visualization, vertical scales of all 1D spectra in all panels were adjusted manually to give approximately the same maximum signal intensities.

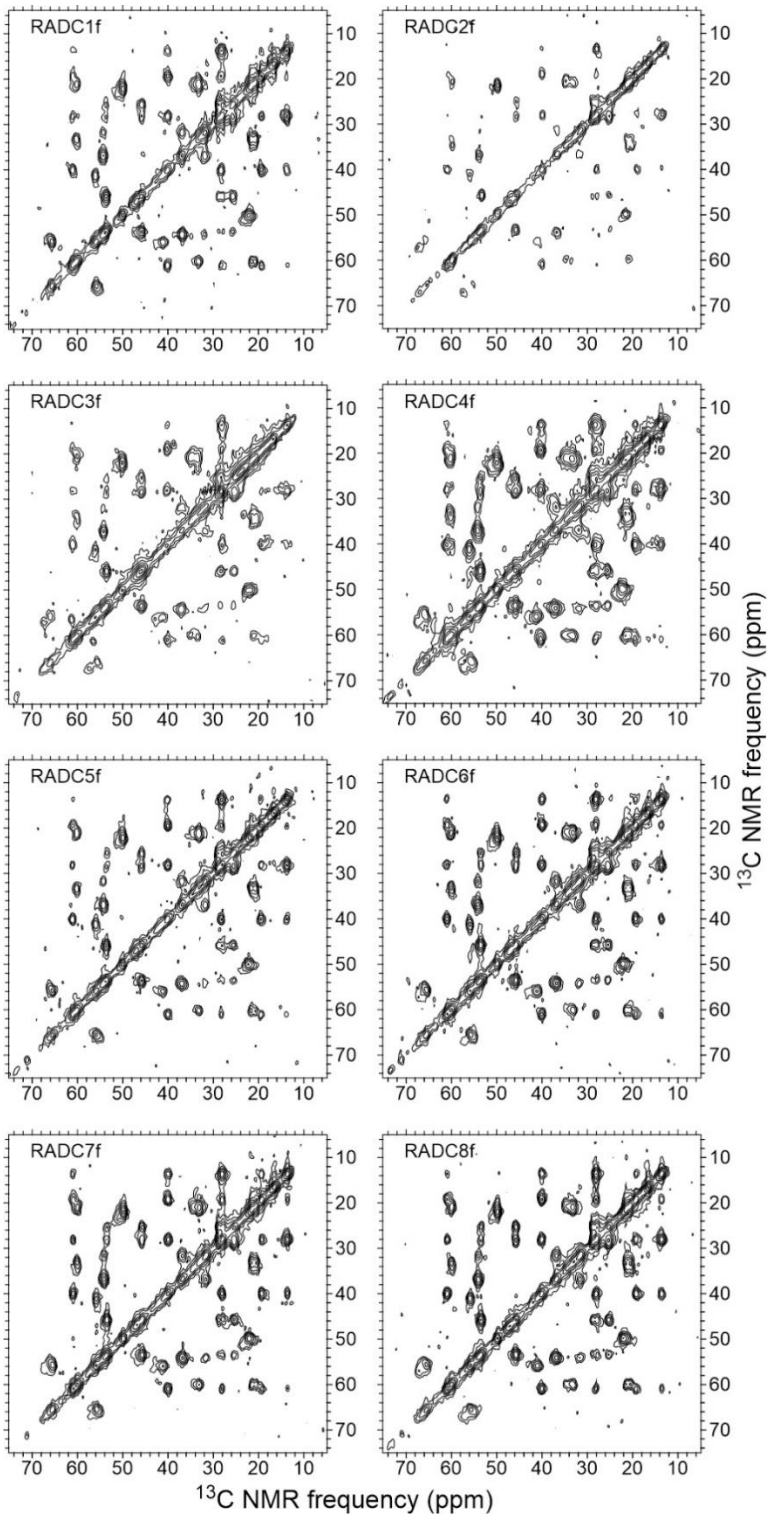


**Figure S4**: 2D $^{13}$C-$^{13}$C solid state NMR spectra of all isotopically labeled Aβ40 fibrils derived from RADC tissue samples. Contour levels increase by successive factors of 2.0, with the lowest contour at approximately 3.0 times the root-mean-squared (rms) noise level in each spectrum.

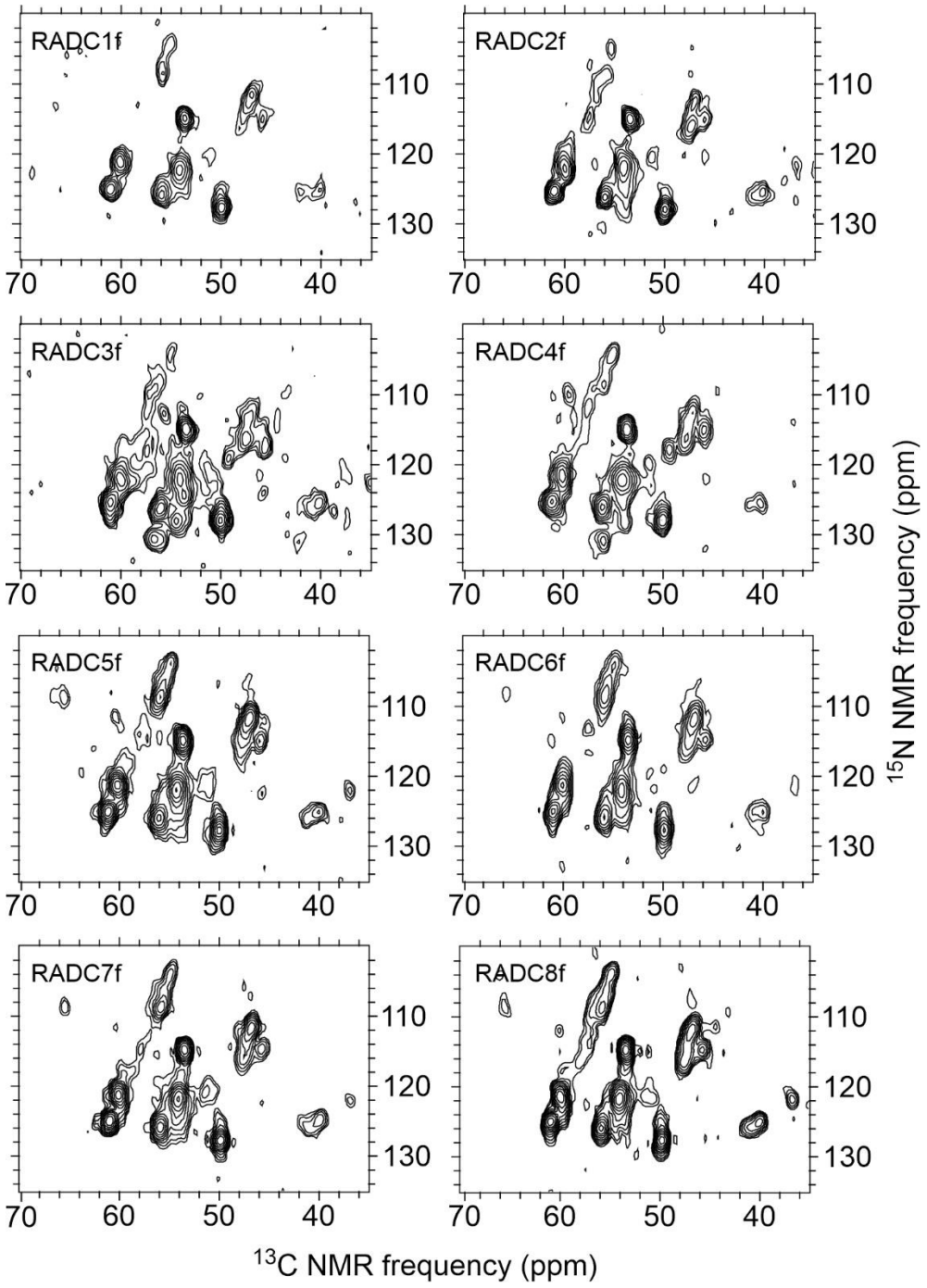


**Figure S5**: 2D $^{15}$N-$^{13}$C solid state NMR spectra of all isotopically labeled Aβ40 fibrils derived from RADC tissue samples. Contour levels increase by successive factors of 1.5, with the lowest contour at approximately 3.0 times the root-mean-squared (rms) noise level in each spectrum.

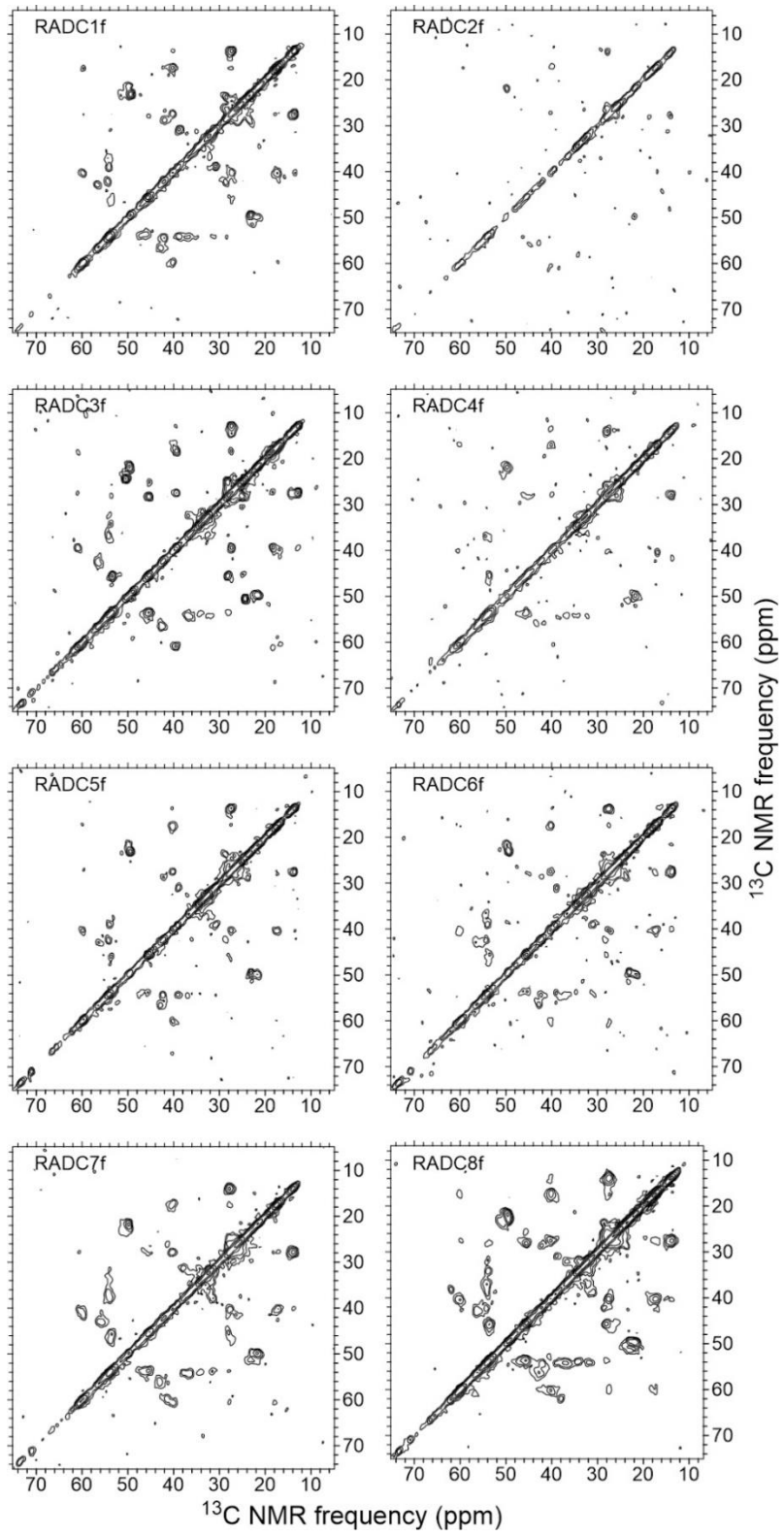


**Figure S6**: Same as Fig. S4, but for Aβ42 fibrils.

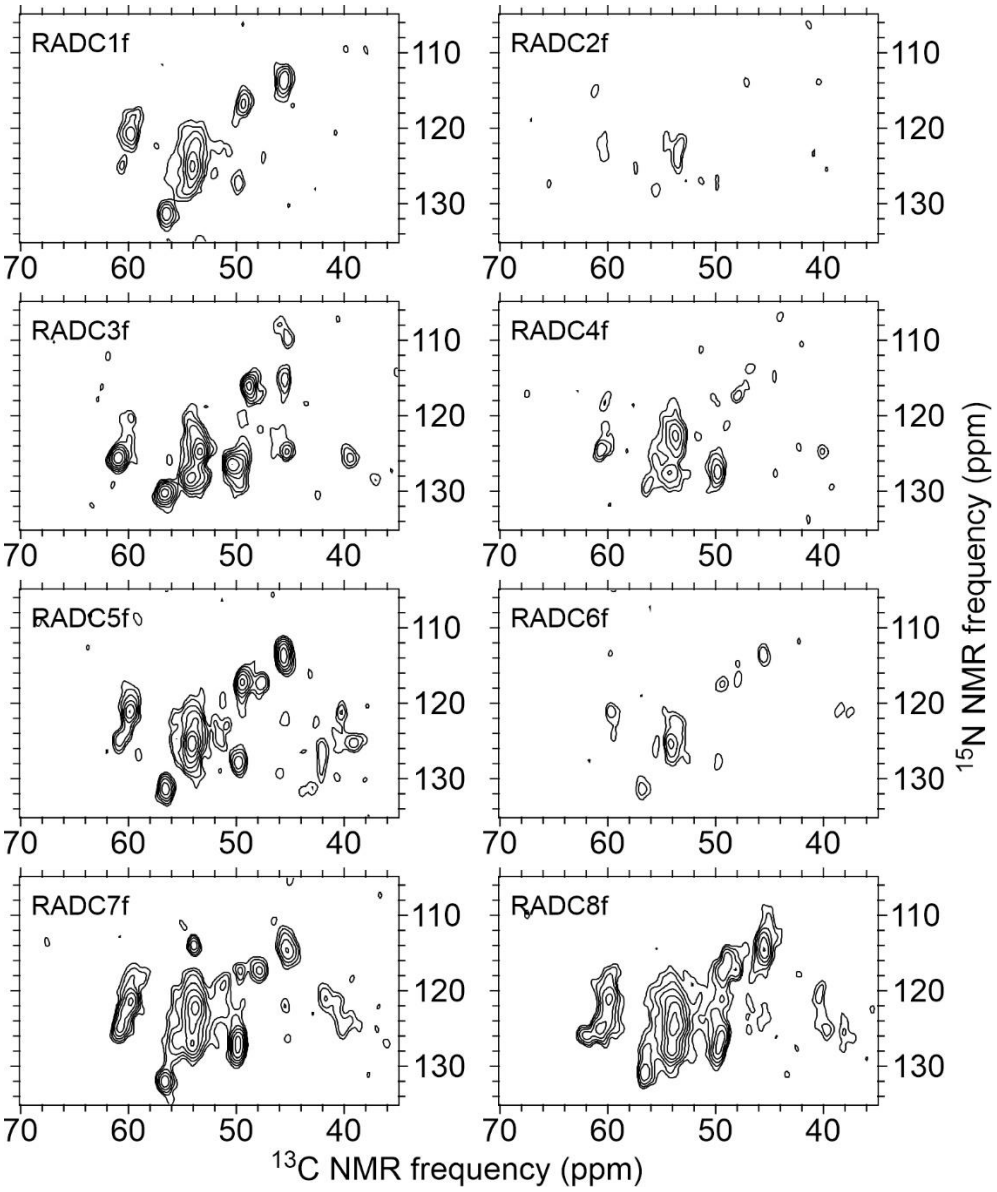


**Figure S7**: Same as Fig. S5, but for Aβ42 fibrils.

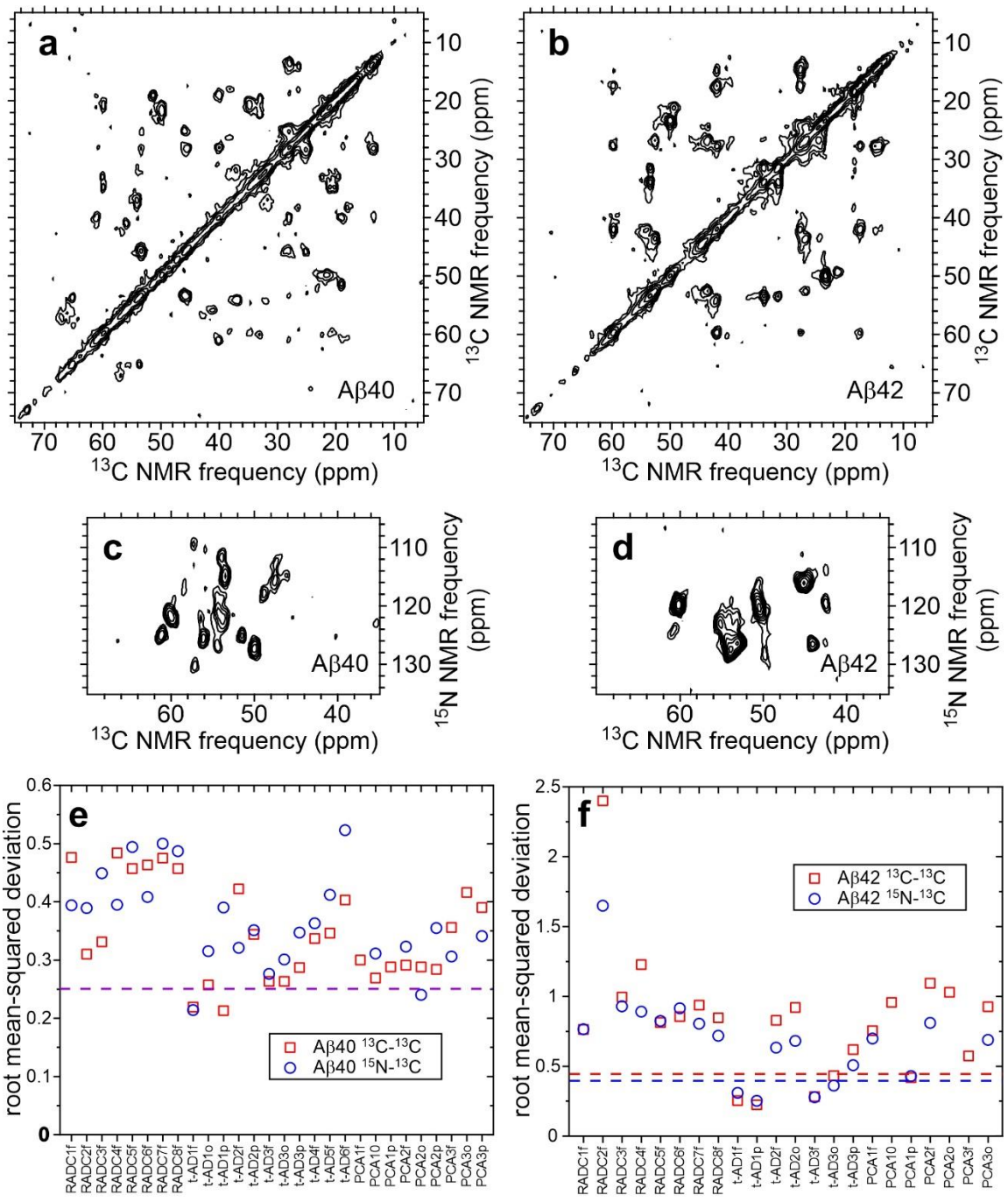


**Figure S8**: Control experiments with fibrils grown in the presence of occipital lobe extract without detectable amyloid. Although TEM measurements after 4 h of incubation showed no seeded fibril growth, fibrils formed spontaneously during longer incubation periods [see Extended Data Figure 4 of Qiang et al. (2)]. (a,b) 2D $^{13}$C-$^{13}$C spectra, plotted as in Fig. S4. (c,d) 2D $^{15}$N-$^{13}$C spectra, plotted as in Fig. S5. (e,f) RMSD values from comparisons with 2D spectra of RADC, t-AD, and PCA-AD fibril samples. Dashed lines indicate RMSD values that correspond to white shades in heat map plots in Fig. 4.

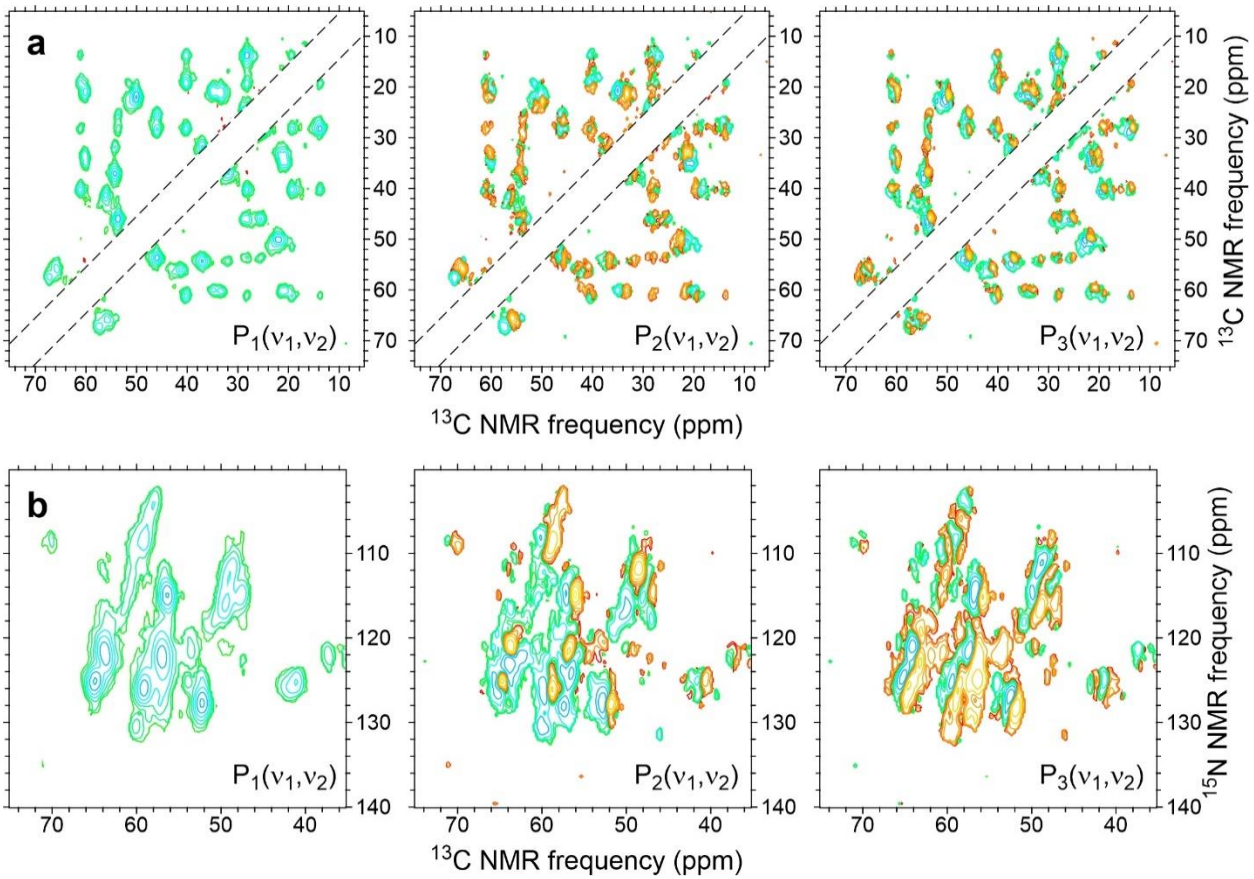


**Figure S9**: Principal component spectra for Aβ40 fibrils. (a) The first three principal component spectra, generated by principal component analysis of all 2D $^{13}$C-$^{13}$C solid state NMR spectra of Aβ40 fibrils derived from RADC, t-AD, and PCA tissue samples (28 spectra). Positive and negative crosspeak intensities in the principal component spectra are indicated by green-blue and red-yellow contours, respectively. Contour levels increase by successive factors of 2.0. Diagonal regions between dashed lines were not included in the principal component analysis. (b) Same as panel a, but for 2D $^{15}$N-$^{13}$C solid state NMR spectra of Aβ40 fibrils (25 spectra).

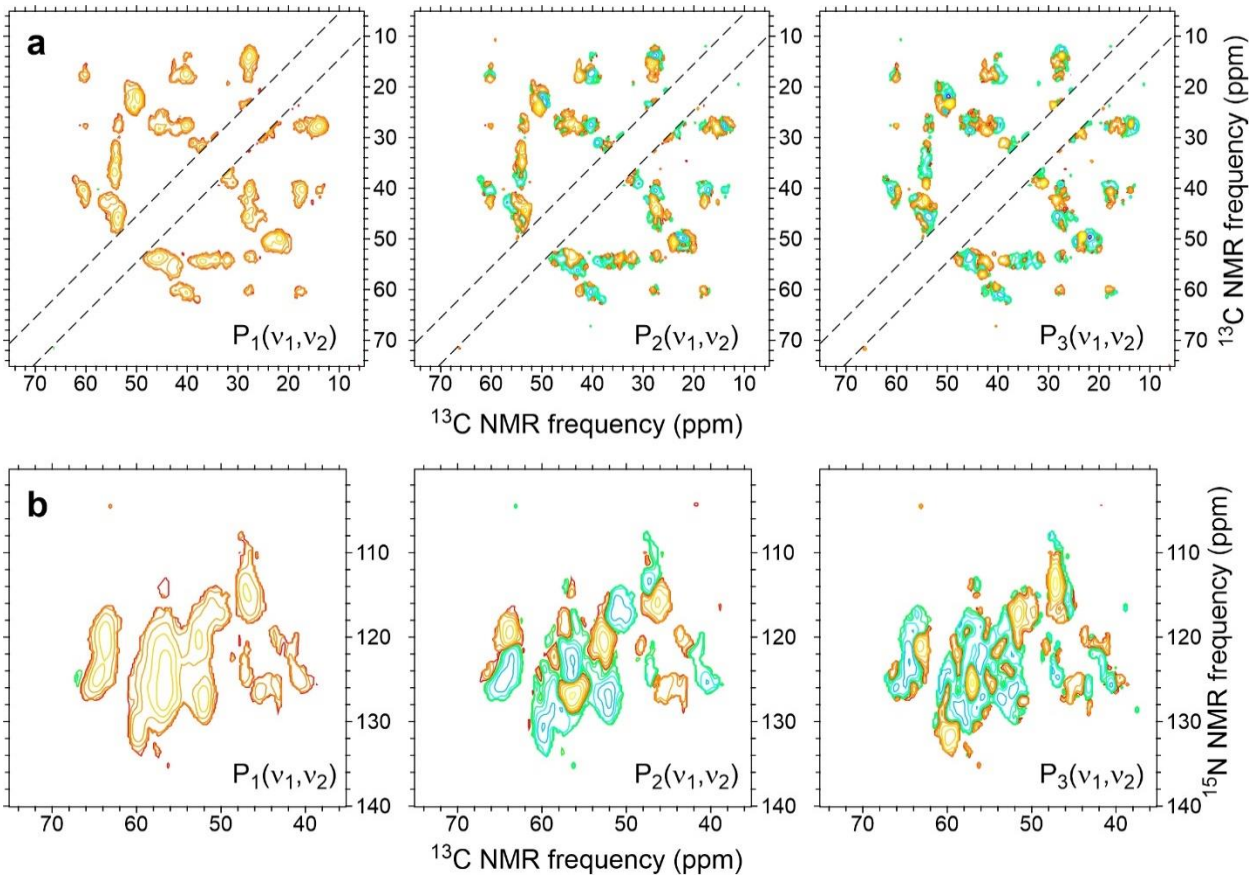


**Figure S10**: Same as Fig. S9, but for Aβ42 fibrils (22 spectra analyzed in panel a, 19 spectra analyzed in panel b).

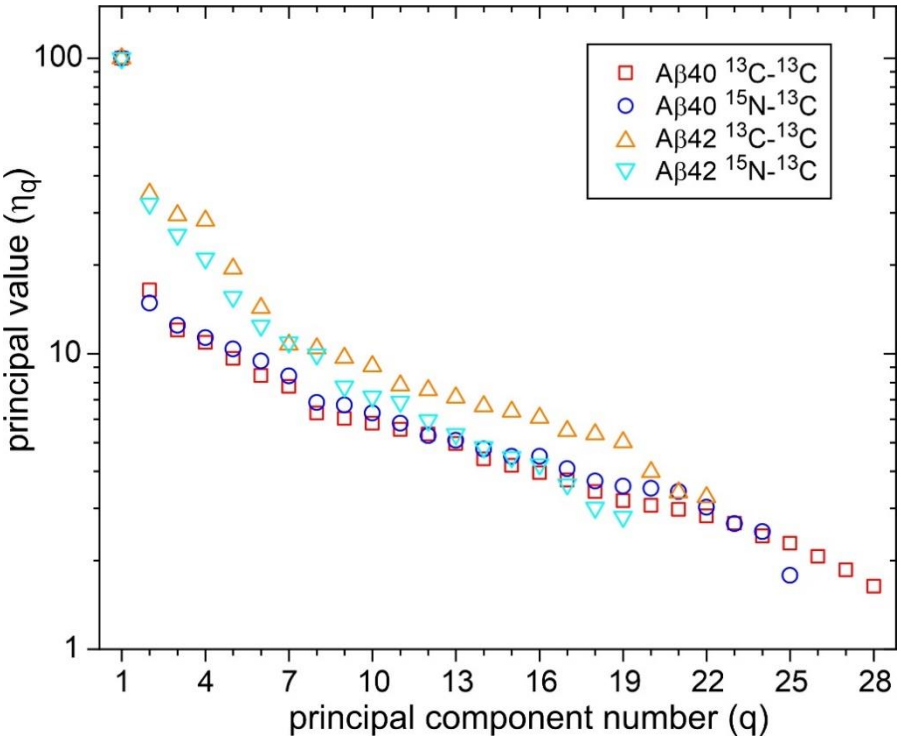


**Figure S11**: Principal values for principal component spectra of brain-derived Aβ40 and Aβ42 fibrils.